Geodetic Imaging of the Coseismic and Early Postseismic Deformation from the 2019 M_w 7.1 and M_w 6.4 Ridgecrest Earthquakes in California with SAR

Eric Fielding[1], Mark Simons[2], Oliver Stephenson[3], Minyan Zhong[3], Sang-Ho Yun[4], Cunren Liang[3], Simran Sangha[5], Zachary Ross[3], Mong-Han Huang[6], and Benjamin Brooks[7]

[1]Jet Propulsion Laboratory, California Institute of Technology
[2]CALTECH
[3]California Institute of Technology
[4]Jet Propulsion Laboratory
[5]NASA Jet Propulsion Laboratory
[6]University of Maryland, College Park
[7]US Geological Survey

November 25, 2022

Abstract

The 4 July 2019 Mw 6.4 Earthquake and 5 July Mw 7.1 Earthquake struck near Ridgecrest, California. Caltech-Jet Propulsion Laboratory Advanced Rapid Imaging and Analysis (ARIA) project automatically processed synthetic aperture radar (SAR) images from Copernicus Sentinel-1A and -1B satellites operated by the European Space Agency, and products were delivered to the US and California Geological Surveys to aid field response. We integrate geodetic measurements for the three-dimensional vector field of coseismic surface deformation for thee two events and measure the early postseismic deformation, using SAR data from Sentinel-1 satellites and the Advanced Land Observation Satellite-2 (ALOS-2) satellite operated by Japanese Aerospace Exploration Agency. We combine less precise large-scale displacements from SAR images by pixel offset tracking or matching, including the along-track component, with the more precise SAR interferometry (InSAR) measurements in the radar line-of-sight direction and intermediate-precision along-track InSAR to estimate all three components of the surface displacement for the two events together. InSAR coherence and coherence change maps the surface disruptions due to fault ruptures reaching the surface. Large slip in the Mw 6.4 earthquake was on a NE-striking fault that intersects with the NW-striking fault that was the main rupture in the Mw 7.1 earthquake. The main fault bifurcates towards the southeast ending 3 km from the Garlock Fault. The Garlock fault had triggered slip of about 15 mm along a short section directly south of the main rupture. About 3 km NW of the Mw 7.1 epicenter, the surface fault separates into two strands that form a pull-apart with about 1 meter of down-drop. Further NW is a wide zone of complex deformation. We image postseismic deformation with InSAR data and point measurements from new GPS stations installed by the USGS. Initial analysis of the first InSAR measurements indicates the pull-apart started rebounding in the first weeks and the main fault had substantial afterslip close to the epicenter where the largest coseismic slip occurred. Slip on a NE-striking fault near the northern end of the main rupture in the first weeks, in the same zone as large and numerous aftershocks along NE-striking and NW-striking trends shows complex deformation.

AGU Fall 2019
S31G-0484

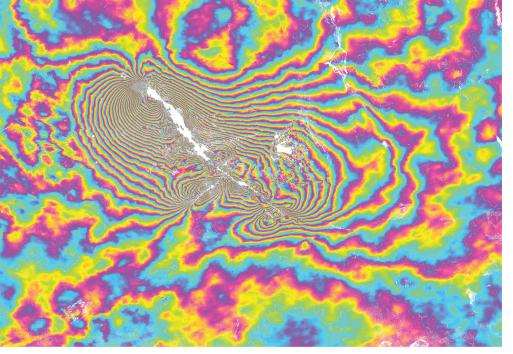

Geodetic Imaging of the Coseismic and Early Postseismic Deformation from the 2019 Mw 7.1 and Mw 6.4 Ridgecrest Earthquakes in California with SAR

National Aeronautics and Space Administration

Eric J. Fielding[1], Mark Simons[2], Oliver Stephenson[2], Minyan Zhong[2], Sang-Ho Yun[1], Cunren Liang[2], Simran Sangha[1], Zachary Ross[2], Mong-Han Huang[3], Benjamin A. Brooks[4]

[1]Jet Propulsion Laboratory, California Institute of Technology, Pasadena, California, USA; [2]Seismological Laboratory, California Institute of Technology, California, USA; [3]University of Maryland, College Park, Maryland, USA; [4]USGS Moffett Field, California, USA

Contact: Eric Fielding (Eric.J.Fielding@jpl.nasa.gov)

Abstract

The 4 July 2019 Mw 6.4 Earthquake and 5 July Mw 7.1 Earthquake struck near Ridgecrest, California. Caltech-Jet Propulsion Laboratory Advanced Rapid Imaging and Analysis (ARIA) project automatically processed synthetic aperture radar (SAR) images from Copernicus Sentinel-1A and -1B satellites operated by the European Space Agency, and products were delivered to the US and California Geological Surveys to aid field response. We integrate geodetic measurements for the three-dimensional vector field of coseismic surface deformation for thee two events and measure the early postseismic deformation, using SAR data from Sentinel-1 satellites and the Advanced Land Observation Satellite-2 (ALOS-2) satellite operated by Japanese Aerospace Exploration Agency. We combine less precise large-scale displacements from SAR images by pixel offset tracking or matching, including the along-track component, with the more precise SAR interferometry (InSAR) measurements in the radar line-of-sight direction and intermediate-precision along-track InSAR to estimate all three components of the surface displacement for the two events together. InSAR coherence and coherence change maps the surface disruptions due to fault ruptures reaching the surface. Large slip in the Mw 6.4 earthquake was on a NE-striking fault that intersects with the NW-striking fault that was the main rupture in the Mw 7.1 earthquake. The main fault bifurcates towards the southeast ending 3 km from the Garlock Fault. The Garlock fault had triggered slip of about 15 mm along a short section directly south of the main rupture. About 3 km NW of the Mw 7.1 epicenter, the surface fault separates into two strands that form a pull-apart with about 1 meter of down-drop. Further NW is a wide zone of complex deformation. We image postseismic deformation with InSAR data and point measurements from new GPS stations installed by the USGS. Initial analysis of the first InSAR measurements indicates the pull-apart started rebounding in the first weeks and the main fault had substantial afterslip close to the epicenter where the largest coseismic slip occurred. Slip on a NE-striking fault near the northern end of the main rupture in the first weeks, in the same zone as large and numerous aftershocks along NE-striking and NW-striking trends shows complex deformation.

Data and Methodology

We used C-band (5.6 cm wavelength) SAR from the Copernicus Sentinel-1 satellites, operated by the European Space Agency (ESA), and L-band (24 cm wavelength) SAR from the JAXA ALOS-2 satellite. Two tracks of Sentinel-1 data cover the Ridgecrest rupture. SAR and InSAR processing was done with the InSAR Scientific Computing Environment (ISCE) v2 *[1][2]*, starting with the single-look complex images from ESA and JAXA. Coseismic interferograms were processed at the highest possible resolution with minimal spatial filtering to minimize phase unwrapping problems and better resolve surface ruptures. SAR pixel offset tracking was run on Sentinel-1 images at full resolution (2.3 meters across track and 14 meters along track) with 200 m matching window chip. Stack processing with ISCE. Time-series analysis done with MintPy *[3]*.

Coseismic Deformation ALOS-2

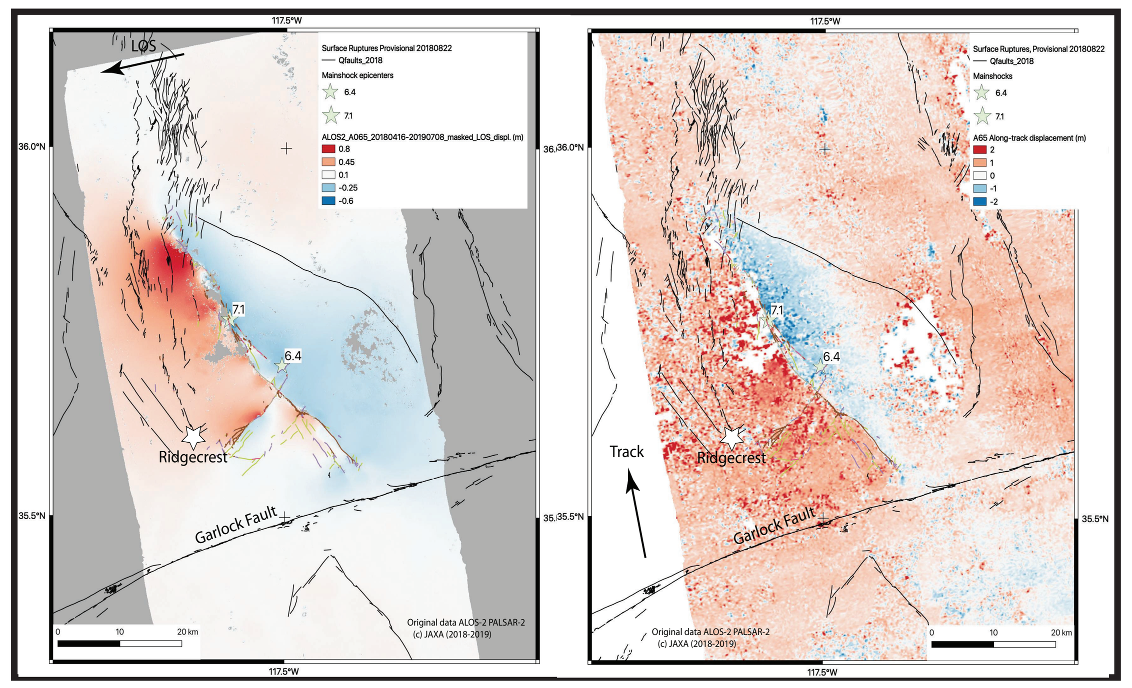

Figure 1. ALOS-2 interferograms from path A65 converted to displacements in meters: (left) standard line-of-sight displacements from pair 2018/04/16–2019/07/08, (right) along-track displacements (MAI) from 2016/08/08–2019/07/08. Overlays are mainshock earthquake epicenters from Z. Ross et al. *[4]*, previously mapped Quaternary Faults (USGS, 2018), and preliminary surface ruptures from Kendrick et al. [5].

Coseismic Deformation Sentinel-1

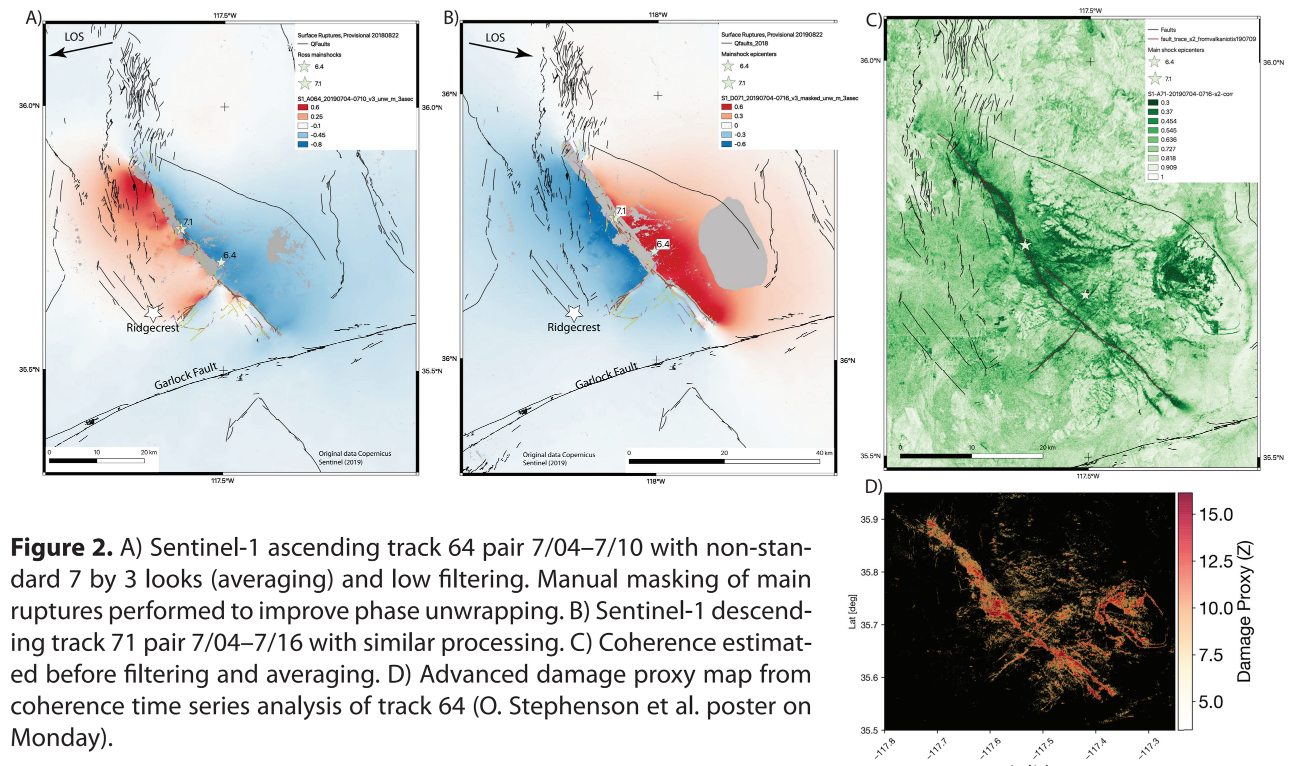

Figure 2. A) Sentinel-1 ascending track 64 pair 7/04–7/10 with non-standard 7 by 3 looks (averaging) and low filtering. Manual masking of main ruptures performed to improve phase unwrapping. B) Sentinel-1 descending track 71 pair 7/04–7/16 with similar processing. C) Coherence estimated before filtering and averaging. D) Advanced damage proxy map from coherence time series analysis of track 64 (O. Stephenson et al. poster on Monday).

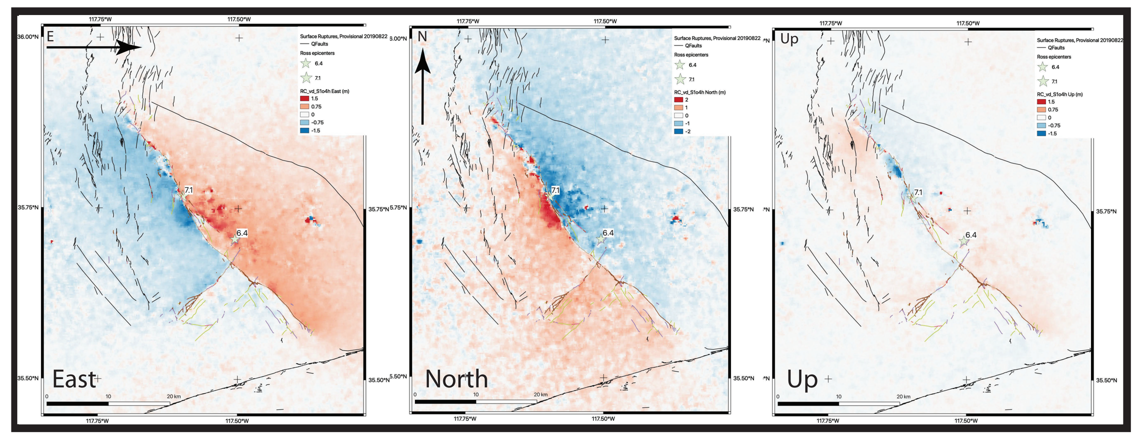

Figure 3. Three components (East, North, Up) of coseismic surface deformation calculated from SAR pixel offset tracking on Copernicus Sentinel-1 images acquired from tracks A64 and D71 (see Fig. 4A). A 500 meter median filter was applied to the offsets. Faults from USGS Qfaults and preliminary ruptures [5] overlain. Note higher noise level on north component due to larger along-track (azimuth) pixel size of Sentinel-1

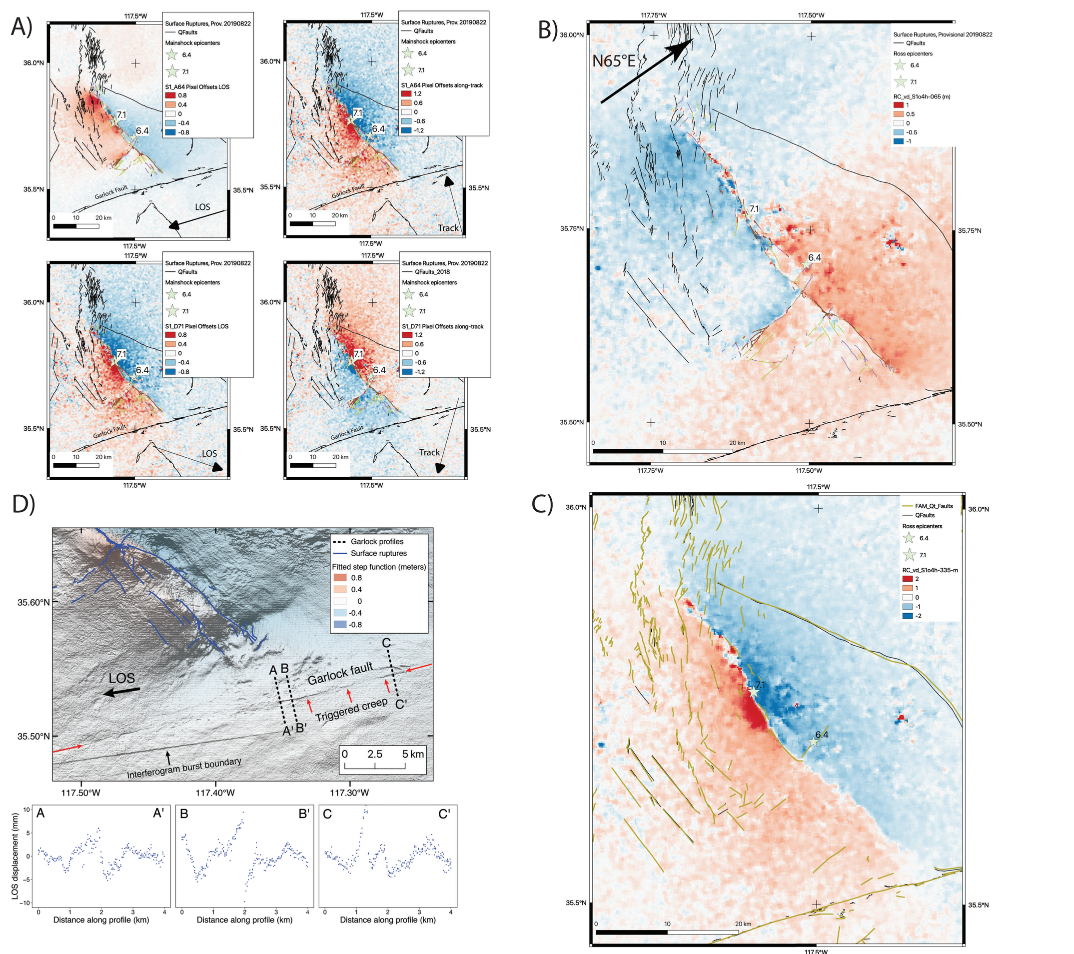

Figure 4. A) Original pixel offset maps from Sentinel-1 in range (line-of-sight) and azimuth (along-track) used for 3D computations. Reprojections of coseismic displacements: B) Horizontal motion in azimuth 65° highlights slip on Mw 6.4 ruptures. C) Horizontal motion in azimuth 335° shows very large strike-slip motion on Mw 7.1 rupture near epicenter. Same faults as in Fig. 3. D) Time-series step-function fit of coseismic deformation using MintPy *[3]* showing shallow triggered slip on Garlock Fault (from *[4]*).

Coseismic data available online:

Fielding, E. J. (2019), Replication Data for: Surface deformation related to the 2019 Mw 7.1 and Mw 6.4 Ridgecrest Earthquakes in California from GPS, SAR interferometry, and SAR pixel offsets, edited, Harvard Dataverse, doi:10.7910/DVN/JL9YMS.

Fielding, E. J., Z. Liu, O. L. Stephenson, M. Zhong, C. Liang, A. Moore, S.-H. Yun, and M. Simons (2020, accepted), Surface deformation related to the 2019 Mw 7.1 and Mw 6.4 Ridgecrest Earthquakes in California from GPS, SAR interferometry, and SAR pixel offsets, Seismol. Res. Lett.

Postseismic Deformation

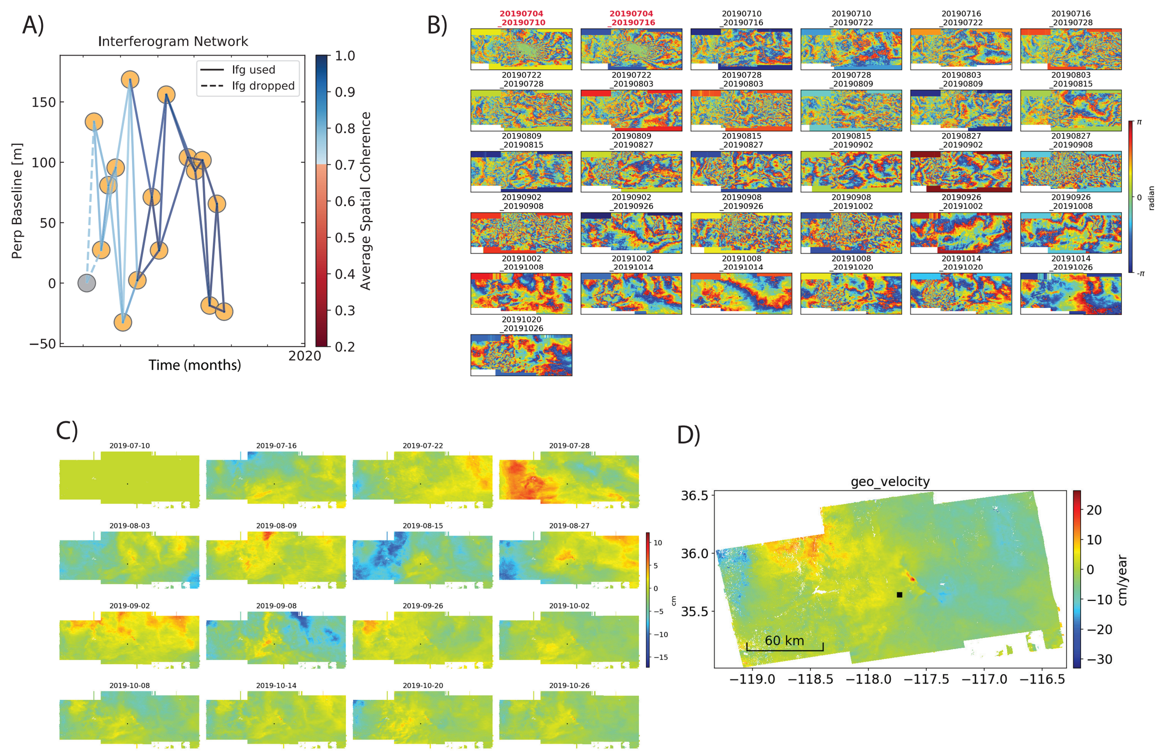

Figure 5. Postseismic time-series analysis with MintPy *[3]* for Sentinel-1 track A64 stack in radar coordinates through 10/26. A) Network of interferograms vs. time, coseismic pairs dropped from postseismic analysis. B) Interferograms rewrapped to original phase. C) Line-of-sight (LOS) displacements of postseismic dates from SBAS inversion relative to 7/10 and reference point marked with square. D) Mean velocity fit to time series after geocoding. No atmospheric corrections applied yet.

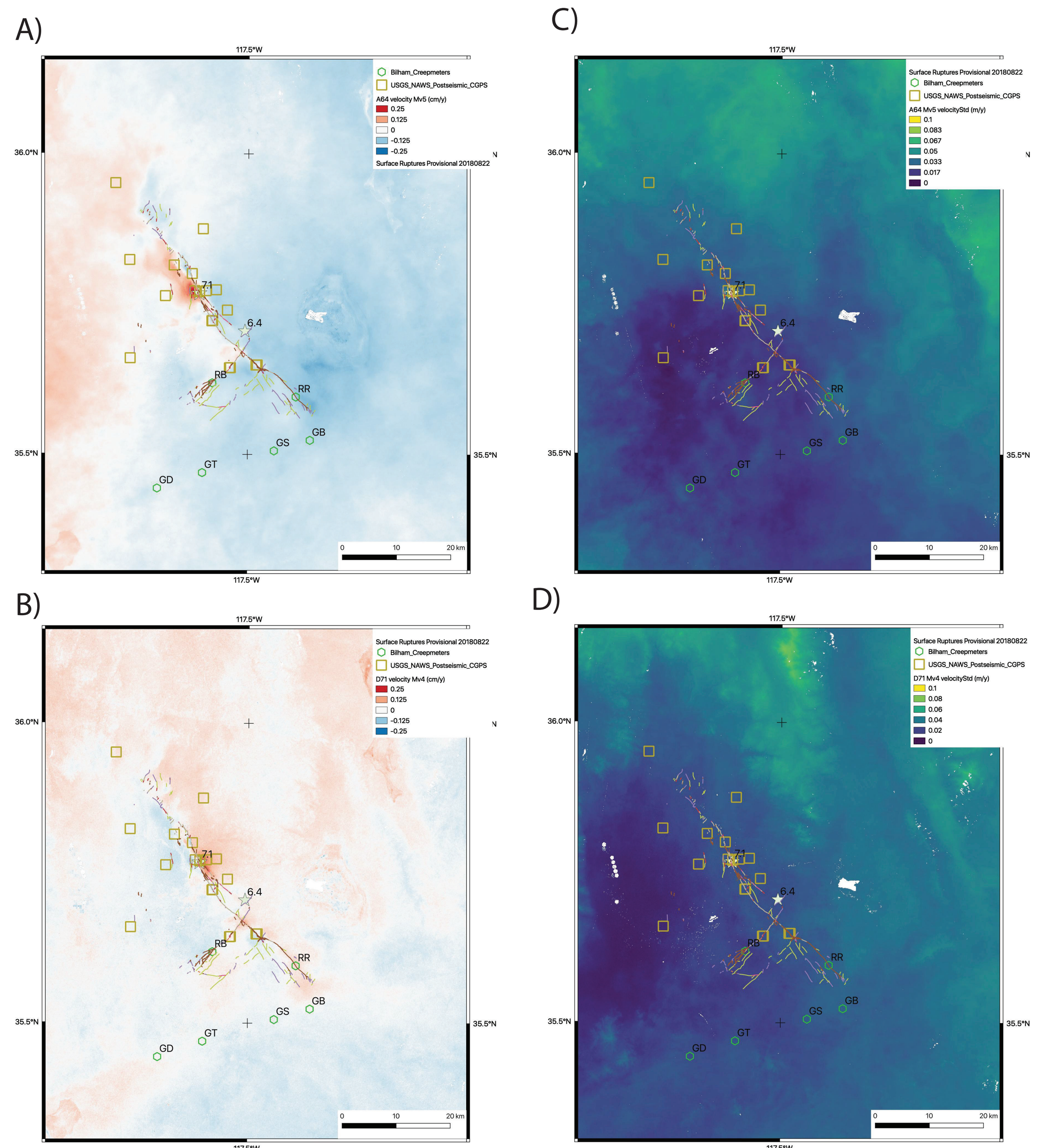

Figure 5. Postseismic time-series mean velocities for Sentinel-1 data through 10/26. A) Mean LOS velocity fit for track A64 with 16 postseismic dates. B) Mean LOS velocity fit for track D71 with 16 postseismic dates. C) Standard deviation of velocity fit for track A64. D) Standard deviation of velocity fits for track D71.

Atmospheric noise is mitigated by the linear velocity fits, but not corrected.

All maps are in meters/year. Overlays are newly mapped coseismic fault ruptures from Kendrick et al. compilation *[5]*, creepmeters installed by R. Bilham, and USGS postseismic GPS stations.

Summary

[1] 2019 Mw 6.4 and Mw 7.1 Ridgecrest Earthquakes on 4 and 6 July ruptured a complex set of faults including two main faults that are orthogonal.

[2] Largest slip during Mw 7.1 earthquake was near epicenter and within 5 km to the south, especially at shallow depths.

[3] Garlock Fault had shallow triggered slip of up to 20 mm (LOS) south of main ruptures.

[4] Postseismic deformation in first four months is dominated by shallow afterslip and poroelastic effects, both strongest near M7 epicenter.

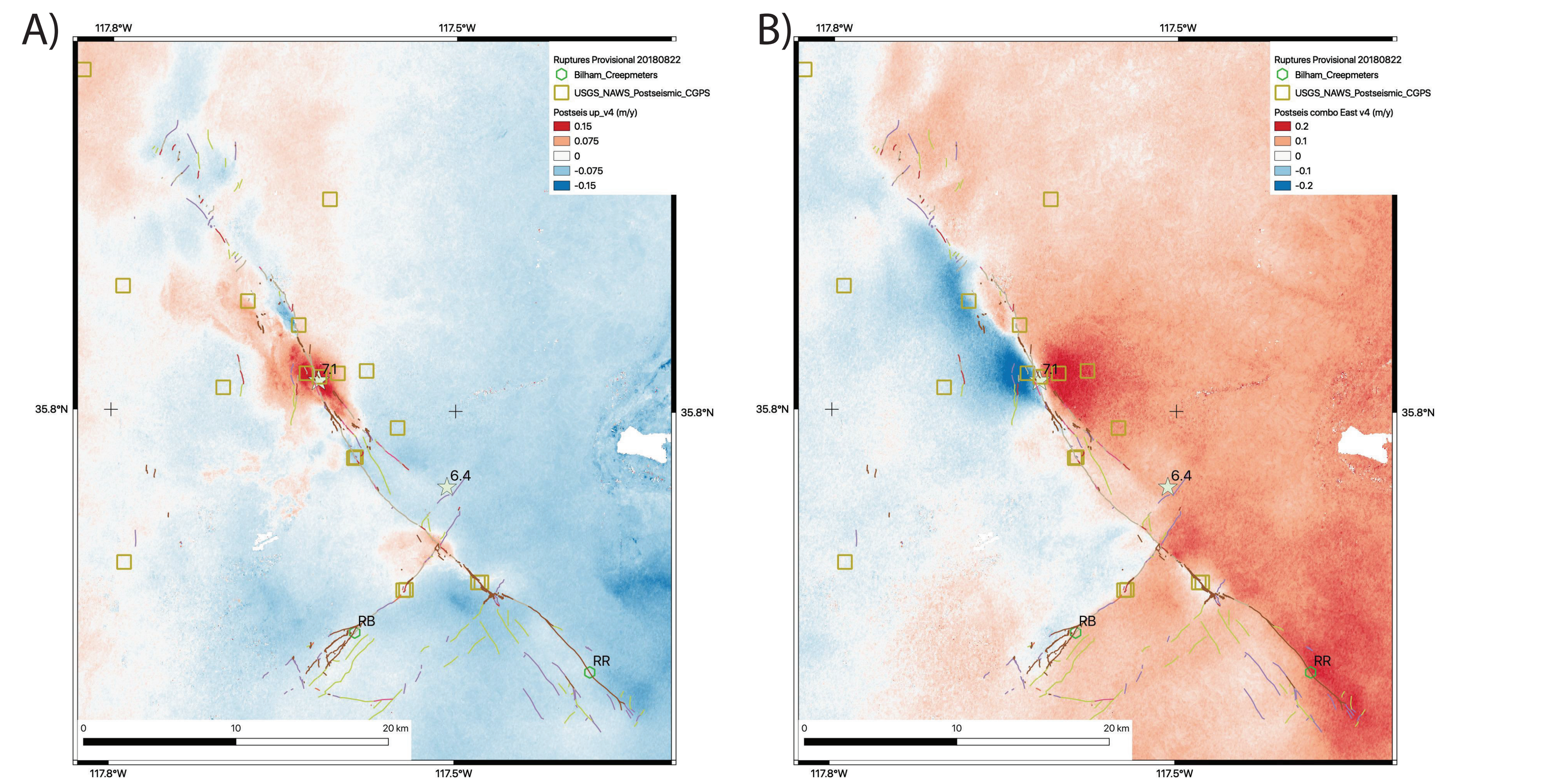

Figure 5. Postseismic time-series mean velocities for Sentinel-1 A64 and D71 data through 10/26 converted to approximate vertical and horizontal deformation components. A) Combination of velocity fits for A64 and D71 to estimate the vertical displacements. This component is largely poroelastic deformation, except for ongoing down-dropping in pull-apart north of M7 epicenter. Large uplift around M7 epicenter is likely due to poroelastic rebound. B) Combination of velocity fits to estimate the horizontal displacements in east direction with north component assumed to be zero. This component enhances the afterslip component of deformation, showing afterslip on many segments of the M7 and M6 earthquake ruptures

Acknowledgments

We thank Zhen Liu, Kate Scharer, Rob Zinke, Gilles Peltzer, Ken Hudnut, and Chris Milliner for valuable discussions. Some figures contain modified Copernicus data, processed by ESA and JPL. Original ALOS-2 radar images are copyright 2016-2019 by the Japan Aerospace Exploration Agency (JAXA) and were provided under JAXA ALOS RA projects. Part of this research was performed at the Jet Propulsion Laboratory, California Institute of Technology under contract with NASA and supported by the Earth Surface and Interior focus area.

References

[1] Rosen, P. A., E. Gurrola, G. F. Sacco, and H. Zebker (2012), The InSAR Scientific Computing Environment, paper presented at 9th European Conference on Synthetic Aperture Radar, Nuremberg, Germany, 23-26 April.

[2] Liang, C., and E. J. Fielding (2017), Measuring Azimuth Deformation With L-Band ALOS-2 ScanSAR Interferometry, *IEEE Transactions on Geoscience and Remote Sensing*, 55(5), 2725-2738, doi:10.1109/TGRS.2017.2653186.

[3] Zhang, Y., H. Fattahi, and F. Amelung (2019), Small baseline InSAR time series analysis: Unwrapping error correction and noise reduction, *Computers & Geosciences*, 133, 104331, doi:10.1016/j.cageo.2019.104331.

[4] Ross, Z. E., Idini, B., Jia, Z., Stephenson, O. L., Zhong, M., Wang, X., Zhan, Z., Simons, M., Fielding, E. J., Yun, S.-H., Hauksson, E., Moore, A. W., Liu, Z., and Jung, J., 2019, Hierarchical interlocked orthogonal faulting in the 2019 Ridgecrest earthquake sequence: *Science*, v. 366, no. 6463, p. 346-351.

[5] Kendrick et al., (2019, 08). Geologic observations of surface fault rupture associated with the Ridgecrest M6.4 and M7.1 earthquake sequence by the Ridgecrest Rupture Mapping Group. Poster Presentation at 2019 SCEC Annual Meeting.